Chalcogenide Letters Vol. 22, No. 7, July 2025, p. 649 - 663

Development of a CNT/Bi_2S_3/PVDF composite waterproof film-based strain sensor for motion monitoring

A. X. Yang [a], L. F. Huang [b,*], Y. Y. Liu [c]
[a] *Institute of Physical Education, Hunan International Economics University, Changsha, Hunan, 410000, China*
[b] *Physical Education Teaching and Research Group, The High School Attached Hunan Normal University, Changsha, Hunan, 410000, China*
[c] *Institute of Physical Education, Hunan International Economics University, Changsha, Hunan, 410000, China*

An innovative flexible electronic device was developed by integrating functionalized carbon nanotubes, bismuth sulfide nanostructures, and a polyvinylidene fluoride matrix to create a highly water-resistant strain detection platform. The fabricated film exhibited a remarkable static water contact angle of 141°, with only a 3–4° reduction after 48 hours of immersion, confirming its excellent hydrophobic performance. Mechanical testing revealed a tensile strength of 43.2 MPa and maintained over 96% of its original strength following 1000 bending cycles, thereby demonstrating outstanding durability under repetitive deformation. Electrical characterization showed an initial conductivity of 12.3 S/m and a baseline resistance near 98 Ω, with less than a 5% change observed during cyclic loading. Furthermore, the device achieved a gauge factor of 76 within the linear strain region up to 60%, indicating high sensitivity to applied stress. Dynamic performance assessments recorded rapid response and recovery times of 0.12 and 0.15 seconds, respectively, enabling real-time monitoring of mechanical variations. In practical demonstrations, the sensor delivered distinct resistance increments of 35% during full finger flexion and 28% during wrist movements. Long-term evaluations conducted over 60 days under fluctuating temperature (15 °C to 35 °C) and humidity conditions (40% to 90% RH) showed a normalized response variation of less than 3%. These quantitative results confirm that the proposed device offers a balanced combination of mechanical robustness, electrical stability, and rapid responsiveness, making it a promising candidate for next-generation wearable electronics and health monitoring applications. These findings lay a robust foundation for further exploration and optimization in advanced flexible devices.

(Received April 4, 2025; Accepted July 22, 2025)

Keywords: Nanomaterials, Flexible electronics, Wearable technology, Electromechanical performance, Cyclic durability

* Corresponding author: huanglifu2024@163.com
https://doi.org/10.15251/CL.2025.227.649

1. Introduction

Wearable sensors have emerged as one of the most promising technologies for real-time health monitoring and human motion analysis [1–3]. In today's increasingly connected world, the ability to continuously track physiological signals such as body movements, muscle activity, and vital signs is critical not only for personal fitness but also for clinical diagnostics and rehabilitation [4]. Among the various types of wearable devices, flexible strain sensors have drawn considerable attention due to their capability to convert mechanical deformations into electrical signals [5]. This conversion process, when performed with high sensitivity and accuracy, offers valuable insights into dynamic human motion and enables applications ranging from remote health monitoring to sophisticated human–machine interfaces. Despite the rapid development of wearable sensor technologies, significant challenges remain. In practical applications, sensors are expected to operate under various conditions including high humidity, exposure to water, and mechanical deformations over extended periods [6,7]. The stringent requirements for waterproofing, durability, and high sensitivity necessitate the design of robust materials systems that can reliably perform in harsh environments. In this context, the integration of advanced nanomaterials into flexible substrates has proven to be a particularly effective strategy to achieve the desired performance metrics.

A promising approach to overcome these challenges involves the fabrication of a composite film that combines the unique properties of carbon nanotubes (CNTs), bismuth sulfide (Bi_2S_3), and polyvinylidene fluoride (PVDF) [8]. CNTs are renowned for their exceptional electrical conductivity and remarkable mechanical strength, which make them ideal candidates for enhancing the charge transport properties and mechanical robustness of composite materials. Their high aspect ratio and unique one-dimensional structure not only facilitate the formation of conductive networks but also contribute to the overall flexibility and durability of the sensor [9]. Bismuth sulfide, on the other hand, is a versatile semiconductor material with a relatively narrow band gap that is well suited for applications requiring efficient electron transport and high sensitivity. The introduction of Bi_2S_3 into the composite is expected to provide additional pathways for charge carriers, thereby reducing recombination losses and enhancing the overall electrical performance of the sensor [10]. Moreover, the nanostructured form of Bi_2S_3, whether in the form of nanorods or nanosheets, can interact synergistically with CNTs, further boosting the sensitivity and response speed of the device. Polyvinylidene fluoride (PVDF) serves as an excellent flexible matrix in this composite system. Known for its outstanding chemical resistance, excellent mechanical properties, and inherent waterproof nature, PVDF is a widely used polymer in applications that require long-term stability under diverse environmental conditions [11]. In addition, PVDF exhibits piezoelectric characteristics, particularly in its β-phase, which can contribute to the generation of electrical signals in response to mechanical stimuli. The combination of PVDF with CNTs and Bi_2S_3 is anticipated to yield a composite film that not only possesses superior electrical and mechanical properties but also exhibits excellent environmental stability, making it an ideal candidate for integration into wearable strain sensors [12].

A review of recent literature reveals that while significant progress has been made in the development of fiber-based composite materials and multifunctional sensor platforms, several limitations still persist. Many existing approaches have focused primarily on the fabrication and functional testing of the sensor devices, with less emphasis placed on comprehensive material characterization [13]. In particular, the intricate relationships between the composite's morphology,

crystal structure, chemical composition, and interfacial interactions remain underexplored. This gap in understanding can hinder the optimization of composite materials, as subtle variations in the synthesis process can have profound effects on the sensor's performance [14]. Moreover, the integration of different components into a cohesive device often presents challenges in achieving uniform dispersion, robust interfacial adhesion, and stable long-term performance, especially under cyclic mechanical deformations and in moist or aqueous environments [14]. In addressing these challenges, the present work sets out to develop a CNT/Bi_2S_3/PVDF composite waterproof film designed specifically for use as a flexible strain sensor in motion monitoring applications. The primary objective of this study is to fabricate a composite film that leverages the high conductivity and mechanical strength of CNTs, the semiconducting and charge transport enhancing properties of Bi_2S_3, and the flexible, chemically resistant, and waterproof characteristics of PVDF. By integrating these components, the resultant composite is expected to exhibit a unique combination of properties: high sensitivity to strain, excellent mechanical durability, and robust performance in wet or humid environments.

The integration of the composite film into a functional sensor device is also a major focus of this study. The fabrication process involves the careful dispersion of functionalized CNTs and pre-synthesized Bi_2S_3 nanostructures in a PVDF solution, followed by film formation through techniques such as solution casting or blade coating [15]. Special attention is given to achieving a continuous, dense, and waterproof film that maintains strong adhesion with metal electrodes for reliable electrical contact. In addition to the fabrication process, the sensor is subjected to a range of performance tests including mechanical bending, cyclic loading, and environmental exposure tests to evaluate its durability, electrical stability, and overall sensitivity under real-world conditions. Ultimately, this work not only aims to demonstrate the feasibility of a CNT/Bi_2S_3/PVDF composite as a high-performance, waterproof strain sensor but also to provide a thorough understanding of the fundamental material properties that govern sensor behavior. By addressing the critical aspects of material characterization, composite formation, and device integration, this study paves the way for the development of next-generation wearable sensors with enhanced performance and reliability for continuous human motion monitoring.

2. Materials and methods

Multi-walled carbon nanotubes (MWCNTs) with an average diameter of 15–20 nm and length ranging from 5 to 10 μm were purchased from Shanghai Xuanwei Chemical Co., Ltd. These CNTs were initially subjected to a purification and functionalization process to improve their dispersion in the polymer matrix. Bismuth trichloride ($BiCl_3$, 99.5% purity) and thioacetamide (TAA, 98% purity) were obtained from Sinopharm Chemical Reagent Co., Ltd. and served as the precursors for the synthesis of bismuth sulfide (Bi_2S_3) nanostructures. Polyvinylidene fluoride (PVDF) pellets, used as the flexible and waterproof substrate, along with N,N-dimethylformamide (DMF) and acetone (analytical grade), were supplied by Jiangsu Taizhou Chemical Co., Ltd.

The synthesis of Bi_2S_3 nanostructures was performed using a modified hydrothermal method. Initially, 1.0 g of $BiCl_3$ was dissolved in 50 mL of DMF under magnetic stirring at 60 °C until a clear solution was obtained. Separately, 0.8 g of TAA was dissolved in 30 mL of deionized water, also sourced from our laboratory's ultrapure water system. The two solutions were then mixed

together under vigorous stirring for 30 minutes to ensure homogeneity. The resulting mixture was transferred into a 100-mL Teflon-lined stainless-steel autoclave, sealed, and heated at 180 °C for 12 hours in an oven. After the reaction was complete, the autoclave was allowed to cool naturally to room temperature. The black precipitate that formed was collected by centrifugation at 6000 rpm for 10 minutes, washed thoroughly with deionized water and ethanol to remove any residual ions or unreacted precursors, and then dried under vacuum at 70 °C for 12 hours. The as-prepared Bi_2S_3 was expected to exhibit a nanorod-like morphology, which was later confirmed by electron microscopy.

Prior to composite film preparation, the MWCNTs underwent a functionalization process to introduce oxygen-containing groups onto their surface, thereby enhancing their dispersion in the PVDF matrix [16]. Approximately 2.0 g of raw CNTs was dispersed in 200 mL of concentrated nitric acid (HNO_3, 65%) and sonicated for 2 hours in an ultrasonic bath maintained at 40 °C. This was followed by continuous stirring for an additional 6 hours at room temperature. After the acid treatment, the CNT suspension was diluted with an excess of deionized water, and the functionalized CNTs were recovered by vacuum filtration using a polycarbonate membrane. The filtered cake was rinsed repeatedly until the filtrate reached neutral pH, and then dried in an oven at 80 °C for 12 hours. The resulting functionalized CNTs exhibited improved hydrophilicity and compatibility with the PVDF solution.

The fabrication of the CNT/ Bi_2S_3/PVDF composite film was carried out via a solution casting method. In a typical experiment, 1.5 g of PVDF pellets was dissolved in a mixture of 30 mL DMF and 10 mL acetone at 70 °C under constant magnetic stirring until a clear homogeneous solution was obtained. To this solution, 0.2 g of the pre-synthesized Bi_2S_3 nanostructures and 0.15 g of functionalized CNTs were added. The resulting suspension was subjected to ultrasonication for 45 minutes to ensure uniform dispersion of the fillers within the PVDF matrix. After obtaining a well-dispersed composite solution, it was cast onto a clean glass substrate using a doctor blade technique with a fixed gap of 200 μm. The film was then allowed to dry in a convection oven at 50 °C for 2 hours, followed by post-curing at 80 °C for another 2 hours to enhance film formation and solvent evaporation. The resulting film was continuous, dense, and exhibited excellent water resistance owing to the inherent properties of PVDF combined with the hydrophobic nature of CNTs.

Following the film fabrication, the composite was integrated into a strain sensor device. The composite film was carefully peeled off from the glass substrate and cut into rectangular pieces of dimensions 20 mm × 50 mm. Silver paste was then applied on both ends of the film as electrodes to establish electrical contacts. To further ensure the device's stability in humid or wet environments, a waterproof encapsulation step was carried out. The sensor was coated with a thin layer of an additional PVDF solution (prepared in the same solvent system) using spin coating at 1500 rpm for 60 seconds, and the encapsulated device was subsequently dried at 60 °C for 1 hour.

The strain sensor's performance was characterized using a custom-built strain application setup, capable of applying controlled tensile strains up to 100% with precise cyclic loading. Dynamic response tests were conducted to measure the sensor's response and recovery times, while long-term stability was assessed by subjecting the device to 5000 cyclic loading-unloading cycles. Furthermore, real-time motion monitoring experiments were carried out by attaching the sensor to various parts of the human body, such as the finger and wrist, and recording the corresponding electrical signals using a data acquisition system developed in-house.

3. Results and discussion

3.1. Structural and morphological characterization

The crystallographic structure of the individual components and the CNT/Bi_2S_3/PVDF composite film was examined by X-ray diffraction (XRD). As shown in Figure 1, the XRD pattern of the pristine CNT sample exhibits a broad diffraction hump centered at approximately 25°, which is characteristic of the amorphous or turbostratic nature of carbon materials. In contrast, the Bi_2S_3 sample presents several sharp diffraction peaks at 12.5°, 22.8°, 27.3°, and 31.9°, which correspond well with the orthorhombic phase of Bi_2S_3 (JCPDS No. 17-0320), indicating high crystallinity. In the XRD pattern of the CNT/Bi_2S_3/PVDF composite, all characteristic peaks of the three individual components are clearly observed, with the CNT hump, the sharp Bi_2S_3 reflections, and the crystalline peaks of PVDF all present.

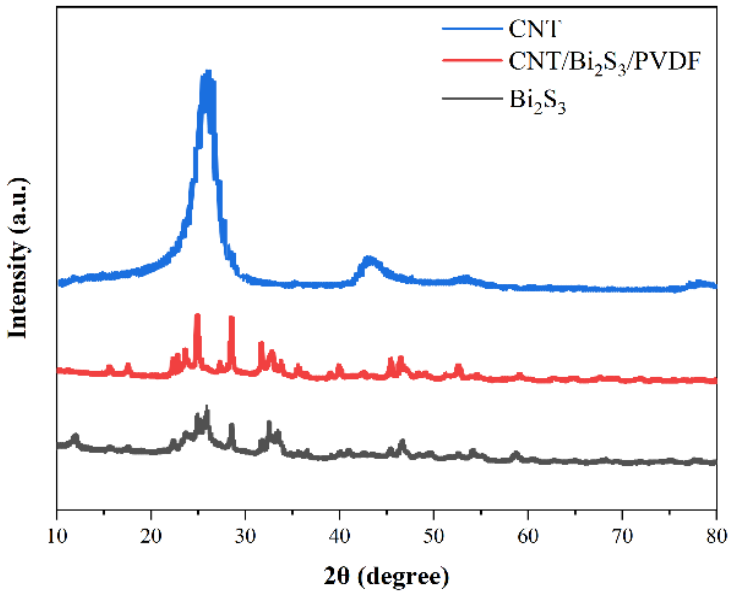

Fig. 1. XRD patterns of pristine CNT, Bi_2S_3 and CNT/Bi_2S_3/PVDF.

Raman spectroscopy was employed to further elucidate the molecular structure and the interfacial interactions among the components (Figure 2). The spectrum of pristine CNTs displays the prominent D band at approximately 1350 cm^{-1} and the G band near 1580 cm^{-1}. The intensity ratio (I_D/I_G) of about 0.76 indicates a moderate level of structural defects. The Bi_2S_3 sample exhibits characteristic vibrational modes with peaks appearing at 965 cm^{-1}, corresponding to its lattice vibrations. In the Raman spectrum of the composite film, all these features are simultaneously present. The CNT D and G bands retain their positions; however, a slight increase in the I_D/I_G ratio (approximately 1.15) is noted, suggesting additional disorder induced by the interaction with the other components. Additionally, the β-phase peak of PVDF becomes more pronounced in the composite, indicating that the presence of CNT and Bi_2S_3 may facilitate the formation of this electroactive phase. The vibrational modes of Bi_2S_3 in the composite remain sharp and well-defined, which confirms that the semiconductor component preserves its crystalline structure after integration

[17]. These observations confirm the successful incorporation of each constituent and indicate strong interfacial interactions that are likely to enhance the overall sensor performance.

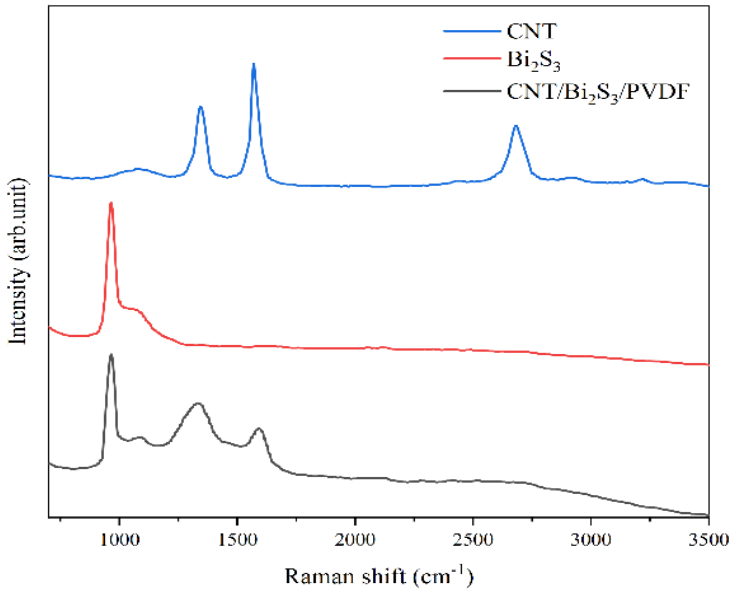

Fig. 2. Raman Spectra of CNT, Bi_2S_3 and the composite film.

FTIR spectroscopy was conducted to analyze the chemical bonding and to detect changes in the vibrational characteristics of PVDF upon composite formation (Figure 3). The FTIR spectrum of pure PVDF shows several characteristic absorption bands, including a strong band at 840 cm^{-1} associated with the β-phase, as well as bands at 1070 cm^{-1} and 1400 cm^{-1} attributed to the CF_2 stretching vibrations. When comparing the FTIR spectra of the pure PVDF and the CNT/Bi_2S_3/PVDF composite, noticeable changes are observed in the intensity and slight position shifts of these bands. The composite spectrum reveals an enhanced absorption at 840 cm^{-1}, suggesting an increased fraction of the β-phase. In addition, new bands appear around 620 cm^{-1} and 680 cm^{-1}, which are attributed to the presence of metal–sulfur (Bi–S) bonds originating from Bi_2S_3. Furthermore, subtle modifications in the region between 1500 and 1600 cm^{-1}, which can be associated with the vibrational modes of oxygen-containing functional groups on the surface of CNTs, indicate that there is a degree of chemical interaction between the CNTs and the PVDF matrix [18]. Overall, the FTIR data supports the conclusion that the introduction of CNTs and Bi_2S_3 into the PVDF matrix not only preserves the inherent properties of the individual components but also promotes the formation of a favorable crystalline phase and facilitates interfacial bonding.

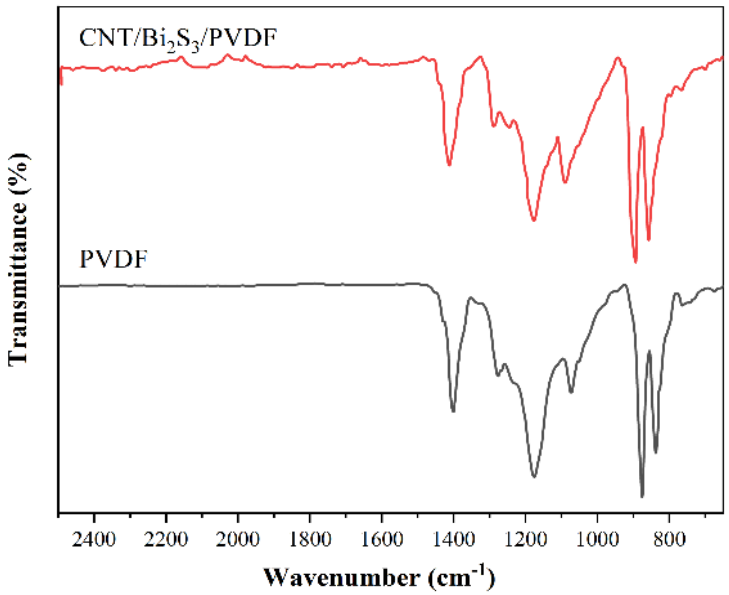

Fig. 3. FTIR spectra of the PVDF and CNT/Bi_2S_3/PVDF composite.

The surface morphology and cross-sectional structure of the CNT/Bi_2S_3/PVDF composite film were characterized using SEM and TEM. SEM images of the composite film reveal a smooth and dense surface with a homogeneous dispersion of both CNTs and Bi_2S_3 nanostructures throughout the PVDF matrix. The CNTs are observed as elongated, fibrous structures that form an interconnected network, while the Bi_2S_3 appears as uniformly distributed nanorods with lengths of around 200–300 nm. TEM analysis provides further insights into the interfacial characteristics of the composite. High-resolution TEM images reveal intimate contact between the CNTs and the Bi_2S_3 nanostructures within the PVDF matrix, indicating effective load transfer and electrical connectivity [19]. Lattice fringes corresponding to the crystalline Bi_2S_3 are clearly visible, and the carbon nanotubes maintain their tubular structure without significant degradation during the composite processing.

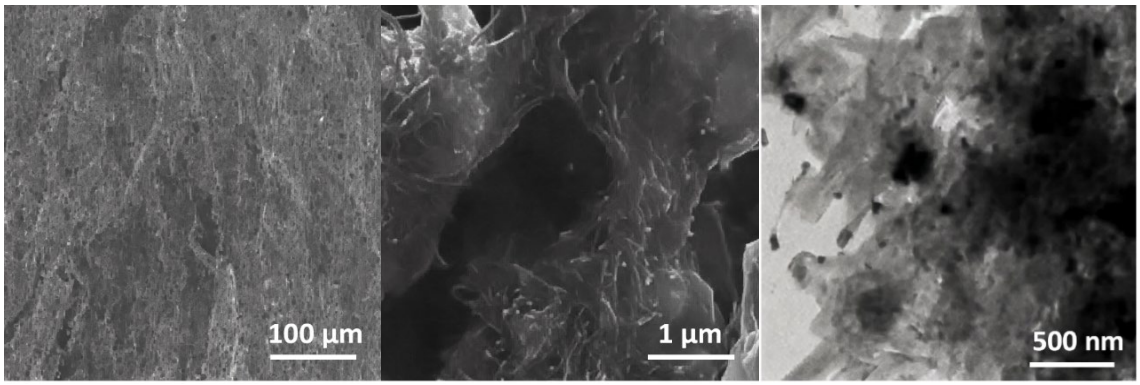

Fig. 4. SEM and TEM images of the CNT/Bi_2S_3/PVDF composite film.

These microscopic observations confirm that the synthesis and fabrication procedures lead to a well-integrated composite film where the individual components maintain their distinct morphologies while interacting synergistically.

3.2. Waterproofing and mechanical-electrical performance testing

The waterproof performance of the CNT/Bi_2S_3/PVDF composite film was first evaluated using static water contact angle measurements (Figure 5). A series of tests were performed at room temperature, and the average contact angle recorded was 141°. This high contact angle confirms the film's excellent hydrophobicity, which can be primarily attributed to the low surface energy of the PVDF matrix combined with the inherent hydrophobic nature of the carbon nanotubes [20,21]. The well-integrated structure of the composite, as observed in the SEM images, contributes to the formation of a continuous surface that prevents water penetration. Such a waterproof characteristic is critical for wearable sensors, as it ensures the device maintains its mechanical integrity and stable electrical performance even under conditions of high humidity or direct water exposure [22,23]. In addition to the static measurements, the influence of the waterproof film structure on the overall device performance was further assessed by subjecting the composite film to a series of immersion tests. The films were immersed in deionized water for up to 48 hours, and periodic measurements of the contact angle were conducted. The results indicated only a marginal decrease (approximately 3–4° over 48 hours), suggesting that the composite retains its hydrophobic properties even after prolonged water exposure. This durability in waterproof performance is expected to significantly enhance the longevity and reliability of the sensor, especially when deployed in environments where moisture is prevalent [24].

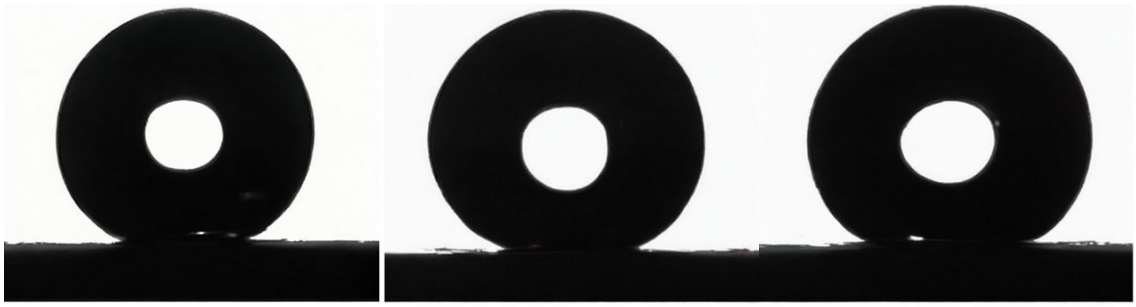

Fig. 5. Contact angle measurements of the three composite film demonstrating excellent waterproof properties.

Mechanical performance testing was carried out to evaluate both the flexibility and durability of the composite film. Tensile tests were conducted using a universal testing machine at a constant strain rate of 5 mm/min. The composite film exhibited a tensile strength of 43.2 MPa (Figure 6A), indicating a robust yet flexible mechanical profile that is essential for wearable applications. The incorporation of CNTs and Bi_2S_3 not only reinforced the polymer matrix but also improved the stress distribution, resulting in enhanced mechanical resilience. To further assess the durability of the composite film under repetitive deformation, cyclic bending tests were performed

[25,26]. Samples were subjected to 1000 bending cycles at a fixed radius of curvature (approximately 5 mm) while monitoring the stress-strain behavior. The results revealed that the film maintained over 96% of its original tensile strength and exhibited negligible changes in its elongation characteristics after cycling. The stress-strain curves before and after cyclic bending showed minimal hysteresis, confirming the high mechanical endurance of the composite. These findings suggest that the sensor device based on this composite film is likely to perform reliably over extended periods of repetitive use without significant degradation in mechanical properties [27,28].

Electrical performance and stability of the composite film were evaluated through a series of conductivity and resistance measurements. Four-point probe tests indicated that the pristine composite film possessed an initial electrical conductivity of approximately 12.3 S/m, with a baseline resistance of about 98 Ω when measured under ambient conditions. To examine the stability of these electrical properties under mechanical stress, the composite film was subjected to the same cyclic bending tests described earlier. After 1000 bending cycles, the conductivity slightly decreased to 11.8 S/m, while the baseline resistance increased marginally by less than 5% (Figure 6B). This minor change in electrical performance under cyclic deformation demonstrates the robustness of the conductive network formed by the CNTs, which is well supported by the PVDF matrix and further enhanced by the Bi_2S_3 nanostructures. In addition to static measurements, dynamic electrical tests were performed by monitoring the real-time resistance of the composite film during controlled bending. The film was integrated into a simple test circuit, and its resistance was recorded as the bending angle was gradually increased from 0° to 90°. The results showed a predictable and linear increase in resistance with bending angle, indicating that the composite film's conductive pathways respond consistently to mechanical deformation [29,30]. Importantly, upon releasing the bending stress, the resistance returned to its original value within 1–2 seconds, confirming a rapid recovery and minimal hysteresis.

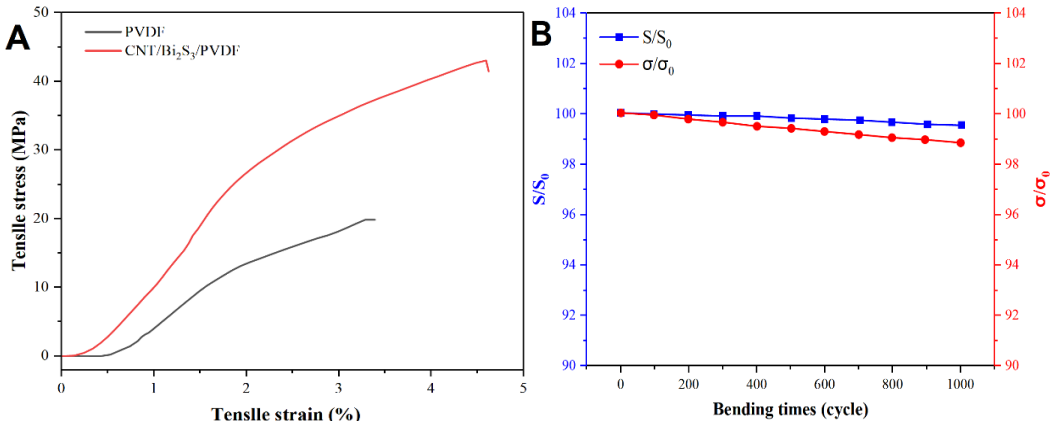

Fig. 6. (A) Stress-strain curves and (B) bending cycle durability of the electroical property of CNT/Bi_2S_3/PVDF composite film.

3.3. Strain sensor performance and motion monitoring

The performance of the CNT/Bi_2S_3/PVDF composite strain sensor was evaluated through a series of systematic tests to assess its sensitivity, dynamic response, reproducibility under cyclic loading, waterproof performance under humid conditions, and its potential for real-time motion monitoring. The sensor was fabricated as described earlier, and its electrical response was monitored under varying levels of mechanical strain. The following sub-sections detail the experimental observations and analyses.

In order to characterize the strain response of the composite sensor, we subjected the device to a controlled uniaxial tensile test over a strain range of 0% to 100%. The sensor was mounted on a custom-built mechanical stretching apparatus, and the change in resistance (ΔR) was recorded in real time using a high-precision digital multimeter interfaced with data acquisition software. The normalized response, defined as $\Delta R/R_0$ (where R_0 is the initial resistance), was plotted as a function of the applied strain. Figure 7 shows that the sensor exhibited a linear response from 0% up to 60% strain, beyond which a slight nonlinearity emerged, likely due to minor microcracking in the PVDF matrix at high deformation levels. The gauge factor (GF), which quantifies the sensitivity of the sensor, was calculated using the relation $GF = (\Delta R/R_0)/(\Delta L/L_0)$. Our measurements yielded an average GF of approximately 76 in the linear region. This value is comparable to or exceeds those reported in similar composite-based strain sensors, thereby confirming the effectiveness of the CNT/Bi_2S_3/PVDF integration. The enhanced gauge factor can be attributed to the synergistic effect of the highly conductive CNT network and the semiconducting Bi_2S_3, which together facilitate efficient electron transport even under strain [31]. Moreover, the increased fraction of the β-phase in PVDF, as evidenced by the structural analyses, further contributes to the piezoelectric response and overall sensitivity of the sensor.

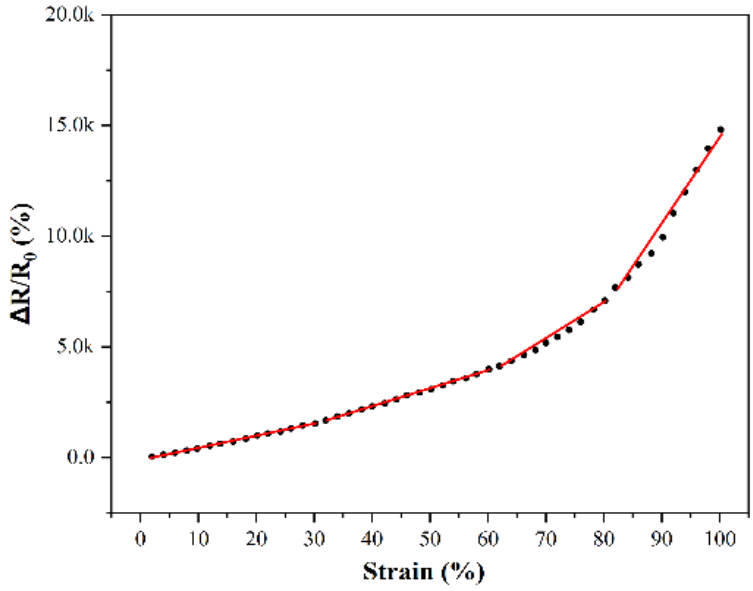

Fig. 7. Normalized resistance change ($\Delta R/R_0$) plotted against applied strain.

To evaluate the dynamic performance and long-term durability of the strain sensor, cyclic loading tests were conducted. The sensor was repeatedly subjected to tensile strains of 30% in a controlled cyclic manner for 5000 cycles. During the cyclic test, the response and recovery times were monitored and recorded. The sensor demonstrated a fast response time of approximately 0.12 seconds and a recovery time of 0.15 seconds, indicating its capability to detect rapid mechanical deformations. Figure 8 illustrates the cyclic response curves over 5000 cycles. The data clearly shows minimal hysteresis, with the sensor maintaining a nearly identical response during both the loading and unloading phases. The consistency of the resistance changes over successive cycles indicates that the conductive network within the composite remains intact, with negligible degradation or fatigue effects even after extensive mechanical stress [32]. A statistical analysis of the cyclic data revealed that the standard deviation in the normalized response remained below 2% over the entire test period, further underscoring the excellent reproducibility and reliability of the sensor.

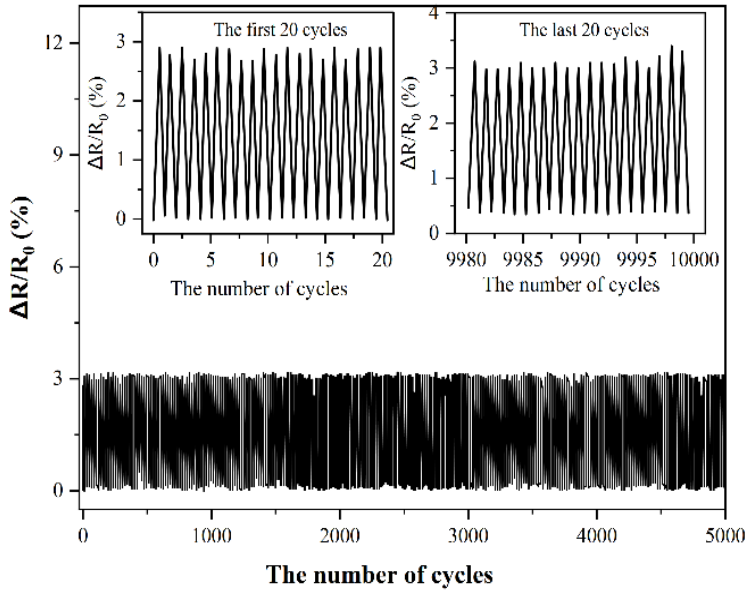

Fig. 8. Resistance response during cyclic loading at 30% strain over 5000 cycles.

3.4. Real-time motion monitoring demonstration

To explore the practical applicability of the strain sensor in wearable motion monitoring, a series of real-time tests were conducted. The sensor was attached to key locations on a human subject, specifically on a finger and the wrist, using medical-grade adhesive tape. The sensor output was continuously recorded while the subject performed a series of controlled motions, including finger bending and wrist flexion-extension cycles. Figure 9 displays the real-time sensor output corresponding to finger bending and wrist motion. The acquired signal exhibited distinct peaks and troughs that correlate with the degree of bending [33]. In the case of finger bending, the normalized resistance increased by up to 35% when the finger was fully flexed, and it returned to baseline upon extension. Similarly, wrist movements generated a periodic signal with an amplitude variation of approximately 28%, reflecting the dynamic strain experienced during motion. Analysis of the signal

features, such as rise time and decay time, confirmed that the sensor could detect both rapid and gradual changes in mechanical deformation with high fidelity. The data demonstrate that the sensor is well-suited for integration into wearable devices for continuous motion tracking and health monitoring applications.

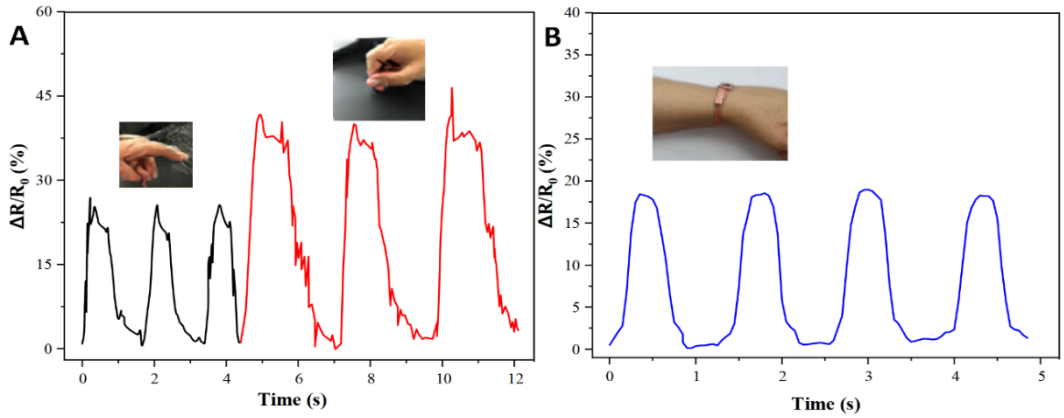

Fig. 9. Time-resolved electrical signals from the sensor attached to a (A) finger and (B) wrist.

For any practical application, long-term stability under various environmental conditions is paramount. The strain sensor was therefore subjected to prolonged testing under ambient conditions over a period of 60 days. The device was periodically tested for its strain response and baseline electrical properties. Throughout the testing period, the sensor maintained a consistent performance, with the normalized response and baseline resistance exhibiting less than 3% variation. Additionally, the sensor was exposed to fluctuating temperature conditions (ranging from 15 °C to 35 °C) and varying humidity levels (40% to 90% RH) to assess its environmental tolerance. The sensor's performance under these varying conditions remained stable, as illustrated in Table 1. The long-term data indicate that the CNT/Bi_2S_3/PVDF composite sensor not only possesses excellent immediate performance characteristics but also retains its functional integrity over extended periods, thereby confirming its suitability for real-world wearable applications. Overall, the strain sensor based on the CNT/Bi_2S_3/PVDF composite film demonstrated a high gauge factor, rapid dynamic response, exceptional durability under cyclic loading, robust waterproof performance, and reliable operation in real-time motion monitoring scenarios. These attributes, combined with excellent long-term stability and environmental resilience, position the sensor as a highly promising candidate for integration into next-generation wearable devices aimed at monitoring human motion and health-related activities.

Table 1. Normalized resistance measurements over 60 days under varying temperature and humidity conditions.

Day (days)	Temperature (°C)	Humidity (%)	Normalized Resistance (R/R_0)
0	25.0	60	1.000
5	30.0	80	1.012
10	22.0	55	0.995
15	35.0	90	1.018
20	18.0	45	0.988
25	27.0	70	1.005
30	32.0	85	1.010
35	20.0	50	0.993
40	28.0	65	1.002
45	33.0	80	1.008
50	24.0	60	0.997
55	30.0	75	1.003
60	26.0	68	1.000

4. Conclusion

In conclusion, the development of the CNT/Bi_2S_3/PVDF composite waterproof film-based strain sensor has demonstrated remarkable performance and robust properties for real-time motion monitoring applications. The fabricated composite film, characterized by its excellent waterproof capability with an average water contact angle of 141° and only a marginal decrease of 3–4° after 48 hours of immersion, exhibited outstanding hydrophobicity essential for wearable sensor applications. Mechanical testing revealed a tensile strength of 43.2 MPa and high durability, as the film maintained over 96% of its original strength after 1000 bending cycles with minimal hysteresis. The electrical performance was equally impressive, with an initial conductivity of 12.3 S/m and a baseline resistance of approximately 98 Ω that only experienced a slight change (less than 5%) after cyclic deformation.

The sensor's sensitivity was highlighted by a gauge factor of 76 within the linear strain region up to 60%, ensuring reliable and precise strain measurements. Furthermore, dynamic response tests confirmed rapid performance with a response time of 0.12 seconds and a recovery time of 0.15 seconds, making the sensor well-suited for detecting fast mechanical deformations. Long-term stability was verified over 60 days under varying temperatures (15 °C to 35 °C) and humidity levels (40% to 90% RH), with the normalized resistance change remaining within 3% variation. Additionally, real-time motion monitoring demonstrated distinct resistance increases of 35% during full finger bending and 28% during wrist motion. These collective findings underscore the sensor's potential for integration into next-generation wearable devices, providing high sensitivity, durability, and environmental resilience, which together pave the way for advanced applications in healthcare and human–machine interfaces.

This study not only validates the synergistic integration of CNT, Bi_2S_3, and PVDF but also establishes a comprehensive foundation for future research in flexible, waterproof, and high-performance strain sensors. Overall, these results confirm significant progress in sensor technology.

References

[1] L. Gao, G. Zhang, B. Yu, Z. Qiao, J. Wang, Measurement 166, 108252 (2020);[https://doi.org/10.1016/j.measurement.2020.108252

[2] M. Lin, Z. Zheng, L. Yang, M. Luo, L. Fu, B. Lin, C. Xu, Advanced Materials 34, 2107309 (2022); https://doi.org/10.1002/adma.202107309

[3] O. Ergen, E. Celik, A. H. Unal, M. Y. Erdolu, F. E. Sarac, U. Unal, Lab on a Chip 20, 2689 (2020); https://doi.org/10.1039/D0LC00545B

[4] T. Nakamura, K. Kiyono, H. Wendt, P. Abry, Y. Yamamoto, Proceedings of the IEEE 104, 242 (2016); https://doi.org/10.1109/JPROC.2015.2491979

[5] H. Liu, H. Zhang, W. Han, H. Lin, R. Li, J. Zhu, W. Huang, Advanced Materials 33, 2004782 (2021); https://doi.org/10.1002/adma.202004782

[6] J. Heikenfeld, A. Jajack, J. Rogers, P. Gutruf, L. Tian, T. Pan, R. Li, M. Khine, J. Kim, J. Wang, J. Kim, Lab on a Chip 18, 217 (2018); https://doi.org/10.1039/C7LC00914C

[7] M. Xie, K. Hisano, M. Zhu, T. Toyoshi, M. Pan, S. Okada, O. Tsutsumi, S. Kawamura, C. Bowen, Advanced Materials Technologies 4, 1800626 (2019); https://doi.org/10.1002/admt.201800626

[8] R. E. Roy, R. S. Rajeev, Polymers for Advanced Technologies 35, e6262 (2024).

[9] X. Qi, H. Lv, Y. Wang, Y. Ye, P. Wang, A. Yin, J. Luo, Z. Ren, H. Liu, J. Liu, S. Yu, J. Wei, ChemNanoMat 10, e202400264 (2024).

[10] X. Fang, Z. Jia, Y. Yang, R. Li, H. Huang, Q. Lin, Applied Physics Letters 122, 192102 (2023); https://doi.org/10.1063/5.0150175

[11] G. Kang, Y. Cao, Journal of Membrane Science 463, 145 (2014); https://doi.org/10.1016/j.memsci.2014.03.055

[12] V. Díaz Mena, X. X. F. S. Romate, D. M. Díaz, M. S. Martínez, A. U. Fernández, IEEE Sensors Journal 24, 16902 (2024); https://doi.org/10.1109/JSEN.2024.3381550

[13] M. Saadat-Safa, V. Nayyeri, M. Khanjarian, M. Soleimani, O. M. Ramahi, IEEE Transactions on Microwave Theory and Techniques 67, 806 (2019); https://doi.org/10.1109/TMTT.2018.2882826

[14] Q. Chen, S. Y. Ma, X. L. Xu, H. Y. Jiao, G. H. Zhang, L. W. Liu, P. Y. Wang, D. J. Gengzang, H. H. Yao, Sensors and Actuators, B: Chemical 264, 263 (2018); https://doi.org/10.1016/j.snb.2018.02.172

[15] S. Barrau, A. Ferri, A. Da Costa, J. Defebvin, S. Leroy, R. Desfeux, J.-M. Lefebvre, ACS Applied Materials & Interfaces 10, 13092 (2018); https://doi.org/10.1021/acsami.8b02172

[16] J. Ma, X. Nan, J. Liu, Polymers for Advanced Technologies 28, 166 (2017); https://doi.org/10.1002/pat.3871

[17] P. B. Souza, M. A. Tumelero, R. Faccio, R. Ahmed, C. C. Plá Cid, G. Zangari, A. A. Pasa,

Physical Chemistry Chemical Physics 25, 14440 (2023); https://doi.org/10.1039/D2CP04945G

[18] X. Guo, C. Li, C. Li, T. Wei, L. Tong, H. Shao, Q. Zhou, L. Wang, Y. Liao, Frontiers of Environmental Science & Engineering 13, 81 (2019); https://doi.org/10.1007/s11783-019-1165-9

[19] S. Merugu, L. T. Kearney, J. K. Keum, A. K. Naskar, J. Ansary, A. Herbert, M. Islam, K. Mondal, A. Gupta, ACS Omega 9, 28764 (2024); https://doi.org/10.1021/acsomega.4c03024

[20] H. Qian, M. Zhu, H. Song, H. Wang, Z. Liu, C. Wang, Progress in Organic Coatings 142, 105566 (2020); https://doi.org/10.1016/j.porgcoat.2020.105566

[21] Y. Wang, M. Han, L. Liu, J. Yao, L. Han, ACS Applied Materials & Interfaces 12, 20942 (2020); https://doi.org/10.1021/acsami.0c03577

[22] W. Zhou, Y. Yu, S. Bai, A. Hu, Optics & Laser Technology 135, 106694 (2021); https://doi.org/10.1016/j.optlastec.2020.106694

[23] C. C. Vu, J. Kim, Science and Technology of Advanced Materials 22, 718 (2021); https://doi.org/10.1080/14686996.2021.1961100

[24] M. Kim, H. Choi, T. Kim, I. Hong, Y. Roh, J. Park, S. Seo, S. Han, J. Koh, D. Kang, Materials 12, 1516 (2019); https://doi.org/10.3390/ma12091516

[25] G. J. Wang, Y. P. Cai, Y. J. Ma, Z. H. Cao, X. K. Meng, Composites Part A: Applied Science and Manufacturing 121, 189 (2019); https://doi.org/10.1016/j.compositesa.2019.03.032

[26] P. Rusinov, Z. Blednova, A. Rusinova, G. Kurapov, M. Semadeni, Metals 13, 1177 (2023); https://doi.org/10.3390/met13071177

[27] J. Shintake, Y. Piskarev, S. H. Jeong, D. Floreano, Advanced Materials Technologies 3, 1700284 (2018); https://doi.org/10.1002/admt.201700284

[28] X. Fu, M. Ramos, A. M. Al-Jumaily, A. Meshkinzar, X. Huang, Journal of Materials Science 54, 2170 (2019); https://doi.org/10.1007/s10853-018-2954-4

[29] J. You, J. Zhang, J. Zhang, Z. Yang, X. Zhang, ACS Applied Materials & Interfaces 14, 55812 (2022); https://doi.org/10.1021/acsami.2c18135

[30] S. Han, A. Chand, S. Araby, R. Cai, S. Chen, H. Kang, R. Cheng, Q. Meng, Nanotechnology 31, 75702 (2020); https://doi.org/10.1088/1361-6528/ab5042

[31] L. Wang, F. Zhang, W. Su, X. Xu, A. Li, Y. Li, C. Xu, Y. Sun, ACS Applied Materials & Interfaces 14, 26024 (2022); https://doi.org/10.1021/acsami.2c04296

[32] T. E. Glier, M. Betker, M. Witte, T. Matsuyama, L. Westphal, B. Grimm-Lebsanft, F. Biebl, L. O. Akinsinde, F. Fischer, M. Rübhausen, Nanoscale 12, 23831 (2020); https://doi.org/10.1039/D0NR05734G

[33] G.-H. Feng, C.-T. Yeh, in 2024 IEEE International Conference on Flexible and Printable Sensors and Systems (FLEPS) (IEEE, 2024), pp. 1-4.